http://dx.doi.org/10.5012/bkcs.2014.35.4.1169

Biological Toxicities and Aggregation Effects of L-Glycine and L-Alanine Capped ZnS:Mn Nanocrystals in Aqueous Solution

Sanghyun Park, Byungkwan Song, Hoon Young Kong,† Jonghoe Byun,† and Cheong-Soo Hwang*

Department of Chemistry, †Department of Molecular Biology, Institute of Nanosensor and Biotechnology, Center for Photofunctional Energy Materials (GRRC), Dankook University, Gyunggi-do 448-701, Korea
**E-mail: cshwang@dankook.ac.kr*
Received November 4, 2013, Accepted December 29, 2013

In this study, water-dispersible ZnS:Mn nanocrystals were synthesized by capping the surface with conventional and simple structured amino acid ligands: L-Glycine and L-Alanine. The ZnS:Mn-Gly and ZnS:Mn-Ala nanocrystal powders were characterized by XRD, HR-TEM, EDXS, ICP-AES, and FT-IR spectroscopy. The optical properties were measured by UV-Visible and photoluminescence (PL) spectroscopy. The PL spectra for the ZnS:Mn-Gly and ZnS:Mn-Ala showed broad emission peaks at 599 nm and 607 nm with PL efficiencies of 6.5% and 7.8%, respectively. The measured average particle size from the HR-TEM images were 6.4 ± 0.8 nm (ZnS:Mn-Gly) and 4.1 ± 0.5 nm (ZnS:Mn-Ala), which were also supported by Debye-Scherrer calculations. In addition, the degree of aggregation of the nanocrystals in aqueous solutions were measured by a hydrodynamic light scattering method, which showed formation of sub-micrometer size aggregates for both ZnS:Mn-Gly (273 ± 94 nm) and ZnS:Mn-Ala (233 ± 34 nm) in water due to the intermolecular attraction between the capping amino acids molecules. Finally, the cytotoxic effects of ZnS:Mn-Gly and ZnS:Mn-Ala nanocrsystals over the growth of wild type *E. coli* were investigated. As a result, no toxicity was shown for the ZnS:Mn-Gly nanocrystal in the colloidal concentration region from 1 μg/mL to 1000 μg/mL, while ZnS:Mn-Ala showed significant toxicity at 100 μg/mL.

Key Words : ZnS:Mn nanocrystal, Glycine capping, Alanine capping, Cytotoxicity, Aggregation

Introduction

The synthesis of nano-sized low-dimensional semiconductor nanocrystals and their applications have been one of the most attractive research subjects for the last few decades.[1,2] These quantum-confined materials have found many applications in non-linear optics and electronic devices,[3] and more recently, in advanced biomedical areas,[4] due to their unique physical, chemical, and optical properties. Among the most practical examples, transition-metal ion-doped ZnS nanocrystallites such as ZnS:Mn[5] and ZnS:Ni[6] have exhibited both high photo luminescent efficiency and thermal stability at ambient temperature, which are critical properties required for commercial electro-luminescence devices. Significant progress in the preparation methods of such materials has also been made.[7] However, these methods often require very high temperatures and pressures, and even the use of bio-hazardous substances. Some II-VI semiconductor nanocrystals such as CdS[8] and CdSe[9] have been developed for fluorescent labeling agents used in biomedical areas. Although they exhibit much greater photo stability than organic dyes, they showed critical problems when directly applied to detections *in vivo*. First, those semiconductor nanocrystals contain very toxic metal ions like cadmium. In spite of their importance, there are only a handful of studies reported regarding their toxicities or safety in living organisms.[10] Second, since most developed semiconductor nanocrystals were grown in hydrophobic solvents such as *n*-trioctyl phosphine, they are hardly compatible with the mainly hydrophilic biological systems. In this regard, there have been several reports on solubilizing the hydrophobic nanocrystals in water by modification of their surfaces with polar organic molecules. The most commonly cited synthetic scheme for water dispersible nanocrystals uses polar surface capping ligands such as mercaptoethanol[11] and sulfodiisooctyl succinate (AOT) molecules[12] to form a micelle structure with negative charges distributed on the nanocrystal surface. In addition, it was shown that the measured quantum yield of AOT capped ZnS:Mn nanocrystal was increased several times after the surface modification. Previously, some conventional amino acid ligands such as arginine[13] and valine[14] were developed as surface capping agents for manganese ion-doped ZnS nanocrystals. These ligands were found as effective capping agents in the syntheses of nanocrystals with narrow size distribution, which are difficult to achieve in aqueous solution due to the different dissociation constants for ZnS in water.[15] In this study, physical and optical characterizations were carried out on ZnS:Mn nanocrystals capped with L-Glycine and L-Alanine, which are simple structured and bio-friendly amino acids. In addition, a comparative toxicological study was conducted on the ZnS:Mn-Gly and ZnS:Mn-Ala over the growth of *E. coli* bacteria. Finally, in this research, we tried to investigate a relationship between aggregation effects of the nanocrystals in aqueous solvent and the observed biological toxicities.

Experimental

Instrumentation. Presented HR-TEM images in this article were taken by a JEOL JEM 1210 electron microscope with a MAG mode of 1,000 to 800,000 in which the accelerating voltage was 40-120 kV. For the sample preparation, dried nanocrystal powders were dispersed in methanol and placed on carbon-coated copper grids (300 Mesh) followed by drying under vacuum for *ca.* 20 h. In addition, elemental compositions of the nanocrystals were determined by an Energy Dispersive X-ray Spectroscopy (EDXS) collecting unit equipped in the HR-TEM, with a Si (Li) detector in an IXRF 500 system. For optical characterizations, UV-Visible absorption spectra were recorded using a Perkin Elmer Lamda 25 spectrophotometer equipped with a deuterium/tungsten lamp. Solution photoluminescence spectra were obtained by a Perkin Elmer LS-45 spectrophotometer equipped with a 500 W Xenon lamp, 0.275 m triple grating monochrometer, and PHV 400 photomultiplier tube in room temperature condition. The powder XRD pattern diagrams were obtained using Rigaku 300 X-ray diffractometer with Cu Kα (1.54 Å) wavelength light source. ICP-AES elemental analyses were performed by an Optima-430 (Perkin Elmer) spectrometer equipped with an Echelle optics system and segmented array charge coupled device (SCD) detector. To prepare a sample of corresponding amino-acids capped ZnS:Mn nanocrystals, 0.5 mL of the nanocrystal containing solution was mixed with 9.5 mL of concentrated nitric acid over the period of 3 days, after which 0.5 mL of the digested solution was placed in 9.5 mL of nanopure-water. For the surface characterization of the nanocrystals, FT-IR spectra were obtained using a Perkin Elmer spectrophotometer equipped with an attenuated total reflection (ATR) unit. In addition, the presented FT-Raman spectrum was recorded by a Bruker FRA106/s spectrophotometer with a resolution of 1 cm^{-1}. Finally, the distribution and degree of aggregation of the nanoparticles were measured by a hydrodynamic light scattering method using an ELS-8000 spectrophotometer equipped with a 30 mW He/Ne laser light source.

Chemicals and Reagents. All solvents, except deionized water, were purchased from Aldrich (reagent grade) and distilled prior to use. All reactants, including L-Glycine, L-Alanine, $ZnSO_4$, $MnSO_4$, and Na_2S, were purchased from Aldrich and used as received. The *E. coli* K-12 (wild type strain) was purchased from the Korean Culture Center of Microorganisms (KCCM 40939).

Syntheses of Glycine and Alanine Capped ZnS:Mn Nanocrystals. A previously reported method for the aqueous synthesis of other aminoacids capped ZnS:Mn nanocrystals *via* the formation of zinc (II)-amino acid coordinated complexes as reactive intermediates was followed with slight modifications.[14] A 50 mL aqueous solution of $ZnSO_4 \cdot 5H_2O$ (1.44 g, 5 mmol) was slowly added to a 50 mL aqueous solution containing 10 mmol of L-Glycine (for ZnS:Mn-Gly) or L-Alanine (for ZnS:Mn-Ala) and NaOH (0.40 g, 10 mmol) at 5 °C (ice-water bath). The solution was warmed to ambient temperature after 1 h of stirring. Separate from this, $MnSO_4 \cdot H_2O$ (0.02 g, 0.1 mmol) and Na_2S (0.40 g, 5 mmol) were dissolved in 20 mL of 0.01 M HCl. This mixture was subsequently transferred to the flask containing the Zn-amino acid complexes under vigorous stirring. The resulting solution was refluxed for 10 h. Slow cooling to ambient temperature and the addition of ethanol resulted in a yellow-white precipitate at the bottom of the flask. Finally, the obtained solids were separated by centrifuging and decanting the supernatant. The solids were then dried for 24 h in a vacuum oven. The detailed experimental data are summarized in Table 1.

Photoluminescence (PL) Efficiency Measurements. The PL efficiencies for glycine and alanine capped ZnS:Mn nanocrystals were measured and calculated by following the same method reported by Williams *et al*.[16] This method involves calculating a relative quantum efficiency by comparing to that of a standard organic dye molecule,[17] a 0.1 M solution of quinine sulfate in H_2SO_4 (purchased from Fluka) in our case, of which the emission wavelength and absolute quantum yield are known as 550 nm and 0.546 respectively at 22 °C. The excitation wavelengths used for the reference material were fixed at the same with the glycine and alanine capped ZnS:Mn nanocrystals, which were obtained from the UV-Visible absorption spectra for the corresponding nanocrystals. The emission spectra for both standard and comparing nanocrystals were recorded at five different concentrations in aqueous solutions using a PL spectrophotometer. A graph of integrated fluorescence intensity versus absorbance for both samples obtained at different concentrations was plotted and the relative PL efficiency for each amino-acid capped ZnS:Mn nanocrystal was calculated by applying the presented equation:

$$\Phi_x = \Phi_{ST}\left(\frac{Grad_x}{Grad_{ST}}\right)\left(\frac{\eta_x^2}{\eta_{ST}^2}\right)$$

In this equation, Φ represents PL efficiency. The subscript ST and x denote the reference material and the comparing nanocrystal respectively. In addition, 'Grad' means the gradient from the plot of integrated fluorescence intensity versus absorbance, and 'η' indicates the refractive index of the solvent. In fact, the solvent factor was eliminated by using the same solvent (water) for both reference and the nanocrystals.

Batch Culture of *Escherichia coli*. *E. coli* K-12 strain was grown in 10 mL of nutrient broth (beef extract 3 g/L, peptone 5 g/L) with shaking at 37 °C for 16 h, both in the absence and presence of the nanocrystals. The nanocrystal powders were dissolved in the nutrient broth to give a concentration of 20 mg/mL, and this stock solution was used to achieve different concentrations in the bacterial culture (0 to 1000 μg/mL). To plot growth, the turbidity of the culture was checked every 30 min by measuring optical density at 600 nm using Spectra Max M2e microplate reader (Molecular Devices). The study was performed in triplicate.

Statistical Analysis. The data were expressed as means ±

Table 1. Data summary of ZnS:Mn-Gly and ZnS:Mn-Ala nanocrystals

	ZnS:Mn-Gly	ZnS:Mn-Ala
UV/Vis (λ_{max}, nm)	321	320
PL emission wavelengths (nm)	599	607
PL efficiency (%)	6.5	7.8
Mn doapant, ICP-AES (%)	0.3	0.9
Average Particle Sizes HR-TEM (nm)	6.4 ± 0.8	4.1 ± 0.5
FT-IR ν (cm^{-1})	3336(br), 2286(w), 2080(w), 1618(s), 1406(w), 1365(w), 1325(w), 1110(s), 1047(m), 978(w)	3203(br), 2285(w), 2107(w), 1592(s), 1506(m), 1415(m), 1350(w), 1303(w), 1064(s), 979(w)
FT-Raman ν (cm^{-1})	259(s), 346(s), 418(m), 481(w), 670(m), 906(w), 989(s), 1338(m), 1391(w), 2958(w)	266(s), 346(m), 448(w), 530(w), 620(m), 768(w), 850(m), 982(s), 1118(w), 1354(m), 1416(w), 1462(w), 2967(w)

SEM. Results were analyzed with GraphPad Prism statistics software (GraphPad Software, Inc., San Diego, CA, USA). The student's t-test was used to evaluate the statistical differences between the groups. A P value of less than 0.05 was considered statistically significant.

Results and Discussions

The average particle sizes of the corresponding amino acid-capped ZnS:Mn nanocrystals were measured from the HR-TEM images as presented in Figure 1. Even though those images did not clearly show discrete individual particles, we enlarged the images as much as we could and measured about 30 identifiable particles to obtain the average particle sizes for the ZnS-based nanocrystals. In the images, the shapes of the particles are fairly close to spheres. The measured particle sizes are 6.4 ± 0.8 nm (ZnS:Mn-Gly) and 4.1 ± 0.5 nm (ZnS:Mn-Ala), respectively, which are close but slightly bigger than that for the other amino acid-capped ZnS:Mn nanocrystals (3.3 nm on average).[13] To support the measurements through the TEM images, we also performed Debye-Scherrer calculations. In the figures, little agglomerations between the particles were observed due to the evaporation of the water and alcohol mixture solvents during the sample preparation. However, the appearance of distinct lattice planes in the fringe images with 2.7 Å lattice spacing indicate that the obtained solids are made of single crystals rather than poly-crystalline aggregates for all the nanocrystal samples.

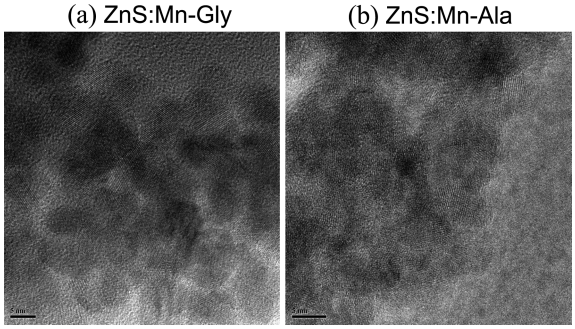

Figure 1. HR-TEM images of: (a) ZnS:Mn-Gly and (b) ZnS:Mn-Ala nanocrystals.

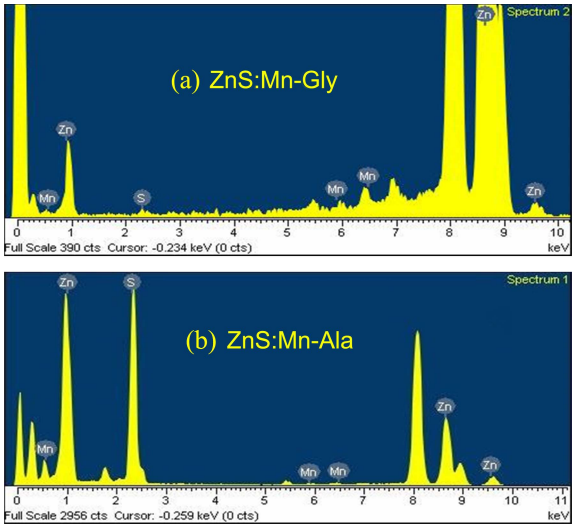

Figure 2. EDXS diagrams of: (a) ZnS:Mn-Gly and (b) ZnS:Mn-Ala nanocrystals.

Figure 2 shows the results of energy dispersive X-ray spectroscopy (EDXS) elemental analysis of the solid products. The presence of zinc, sulfur, and manganese was confirmed in addition to the large amounts of carbon and oxygen atoms in the powder samples. The EDXS analyses showed that the doping percentages of the manganese ions in the measured ZnS:Mn nanoparticles were 0.7% (ZnS:Mn-Gly) and 0.3% (ZnS:Mn-Ala). To determine the doping concentration of metal ions more precisely, Inductively Coupled Plasma-Atomic Emission Spectrometry (ICP-AES) analyses were also performed. Three trials of the sample measurements revealed that the average elemental proportions of the Mn^{2+} ions relative to the ZnS parent crystal were 0.3% (ZnS:Mn-Gly) and 0.9% (ZnS:Mn-Ala), respectively. The manganese (II) ion doping concentration in the ZnS:Mn crystals was intended to be approximately 1.0%, which has been reported as the optimum for PL efficiency for other ligand-capped ZnS:Mn nanocrystals.[15]

The optical properties of the ZnS:Mn-Gly and ZnS:Mn-Ala nanocrystals were measured *via* UV visible and photoluminescence (PL) spectroscopy, as shown in Figures 3 and Figure 4. The PL spectra showed broad emission peaks appeared at 599 nm (ZnS:Mn-Gly) and 607 nm (ZnS:Mn-

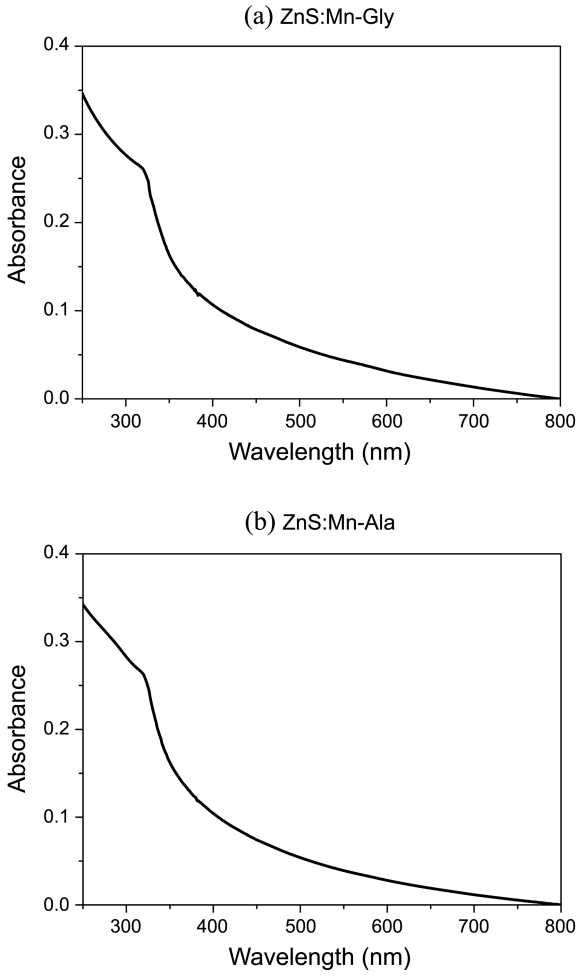

Figure 3. UV-Visible absorption spectra of: (a) ZnS:Mn-Gly and (b) ZnS:Mn-Ala nanocrystals.

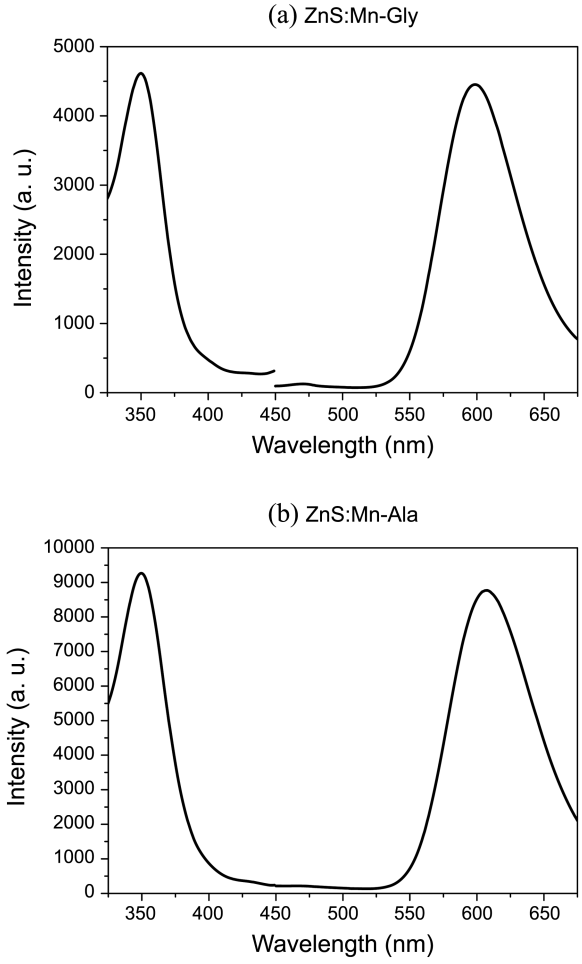

Figure 4. PL emission and excitation spectra of: (a) ZnS:Mn-Gly and (b) ZnS:Mn-Ala nanocrystals.

Ala). The corresponding emission spectra were obtained by fixing the excitation wavelengths at the corresponding UV-Visible absorption peaks of the nanocrystals (Table 1). The dominant absorption shown in the absorption spectra was probably caused by the fundamental band-to-band absorption in the ZnS host,[18] and the increased band gap of the ZnS:Mn nanocrystals (*ca.* 3.87 eV) compared to that for bulk ZnS solid (3.54 eV) is due to the quantum confinement effect for nanosized materials.[19] The yellow-orange light emissions around 600 nm were attributed to the $^4T_1 - {}^6A_1$ transition of Mn^{2+} ions.[20] In the luminescence pathway, if the surface defect states are located close to the conduction band, the direct energy transfer from the ZnS host to the Mn^{2+} activator is significantly interrupted, which can cause weakening in the orange emission as well as enlarging of the Stokes shift.[21] The excitation peaks in Figure 4 were also obtained by fixing the light sources at the obtained corresponding emission wavelengths, and the resulting peaks appeared at 350 nm for both ZnS:Mn-Gly and ZnS:Mn-Ala nanocrystals. The observed large Stokes shifts of approximately 280 nm for the amino acid-capped ZnS:Mn nanocrystals are one of the typical properties for most known transition metal-ion-doped nano-sized crystalline materials.[22] The PL efficiencies for both ZnS:Mn-Gly and ZnS:Mn-Ala nanocrystals were measured and calculated using the method reported by Williams *et al.* as described in the previous experimental section.[16] This method involves calculating the relative quantum yield through a comparison with a standard material, a 0.1 M solution of quinine sulfate in H_2SO_4 (Fluka) in our case, of which the emission wavelength and reported absolute quantum yield are 550 nm and 0.546 (at 22 °C), respectively. The calculated relative PL efficiencies were 6.5% (ZnS:Mn-Gly) and 7.8% (ZnS:Mn-Ala), which are slightly lower than that for L-Valine-capped ZnS:Mn nanocrystal (15.8%),[14] in which the difference in the structure is an isopropyl substituent in the same back bone.

In Figure 5, the wide-angle X-ray diffraction (XRD) patterns of powder samples of the amino acid-capped ZnS:Mn nanocrystals are presented. Although most of the peaks are broad, there were clearly indexable (008), (110), and (118) peaks in the spectra, indicating that all the amino acid-capped ZnS:Mn nanocrystals are in hexagonal wurtzite phases in the space group of $P6_3mc$ (JCPDS 39-1363).[23] In addition, we also performed Debye-Scherrer calculations for ZnS:Mn nanocrystals using the obtained XRD peaks to compare with the particle size measured from the HR-TEM

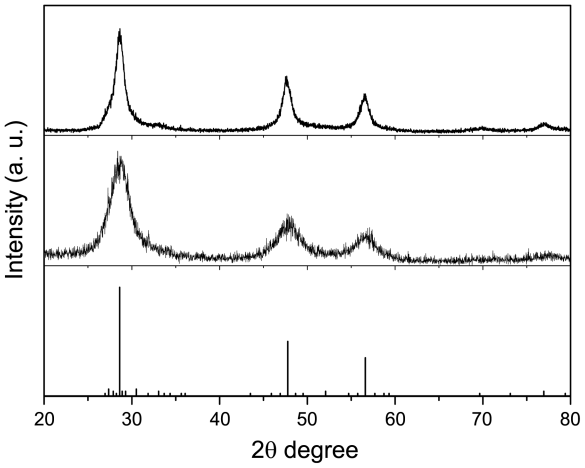

Figure 5. XRD pattern diagrams of: (top) ZnS:Mn-Gly, (middle) ZnS:Mn-Ala, and (bottom) ZnS bulk solid in a wurtzite phase (JCPDS 39-1363).

images.[24] From the measured full width at half maxima (FWHM) of the selected XRD peaks, we obtained the calculated average particle sizes for ZnS:Mn-Gly and ZnS:Mn-Ala nanocrystals as 3.2 nm and 3.9 nm, respectively.

In addition, the corresponding amino acid molecules attached on the surfaces of the ZnS:Mn nanocrystals were characterized by FT-IR and FT-Raman spectroscopy. Figures 6 and 7 present FT-IR and FT-Raman spectra obtained from ZnS:Mn-Gly and ZnS:Mn-Ala nanocrystals, in which peaks obtained from corresponding free amino acids were overlapped for direct comparison. All of the obtained peak data are listed in Table 1, and their assignments are described in Table 2. The overall FT-IR and FT-Raman spectra of the ZnS:Mn-Gly and ZnS:Mn-Ala nanocrystals were found to be quite different from that obtained by corresponding free amino acid molecules. The assignments for the peaks were done by comparing papers regarding assignments for FT-IR and FT-Raman spectra of glycine[25] and alanine[26] using computational methods. For the alanine molecules coordinated onto the ZnS:Mn nanocrystal in the FT-IR spectrum, the peaks that appeared near 2285 cm^{-1} and 1592 cm^{-1} were assigned as asymmetric stretching modes of the zinc-coordinated $-NH_2$ and $-COO^-$ groups of the amino acids, in which the glycine coordinated onto the nanocrystal showed similar peaks at 2286 cm^{-1} and 1618 cm^{-1}. According to the reference literature, those peaks were shifted from that for the corresponding free aminoacids precursors in which asymmetric stretching of NH (2604 cm^{-1}) and COO (1595 cm^{-1}) for L-alanine. These showed a very similar shift pattern for asymmetric stretching peaks of NH (2330 cm^{-1}) and COO (1636 cm^{-1}) from a coordination complex of L-alanine with zinc thiourea sulfate.[27] As shown in Figure 6, these peaks are slightly shifted from that for the free amino acid precursors since they were attached to much heavier transition metal ions.[28] The broad peaks around 3300-3200 cm^{-1} are probably caused by mixed peaks of asymmetric stretching of N-H and C-H moieties. FT-Raman spectra presented in Figure 7 are more useful to assign the peaks that appeared at a lower-frequency region. For the ZnS:Mn-Ala nanocrystal, peaks that appeared at 1462 cm^{-1} and 1416 cm^{-1} were assigned as C-H bending modes. Peaks that appeared at 1338 cm^{-1} (ZnS:Mn-Gly) and 1354 cm^{-1} (ZnS:Mn-Ala) were assigned as overlapped bending modes of the zinc-coordinated NH and COO moieties since those peaks were shifted from that for the free glycine (1380 cm^{-1}) and alanine (1395 cm^{-1}) molecules. Most peaks in the region from 400 to 1100 cm^{-1} for both nanocrystals can be assigned as C-H, C-C, C-N, and C-O bending mode peaks of the corresponding capping amino acid molecules. The peak that appeared at 346 cm^{-1} for both nanocrystals can be assigned as transverse and longitudinal optical phonon of the Zn-S crystal lattice.[29]

Since glycine and alanine-capped water-soluble ZnS:Mn semiconductor nanocrystals were successfully synthesized, their toxic effects in a typical enteric bacterium, *Escherichia coli* (*E. coli*), were also evaluated. By comparing the growth curve of an *E. coli* batch culture in the presence and absence of ZnS:Mn-Gly or ZnS:Mn-Ala, any cytotoxic effects of the nanocrystals could be examined. For these experiments, the optical density (OD) 600 method was employed, which measures the degree of turbidity of the nutrient broth by filling with growing bacteria.[30] The more turbid solution

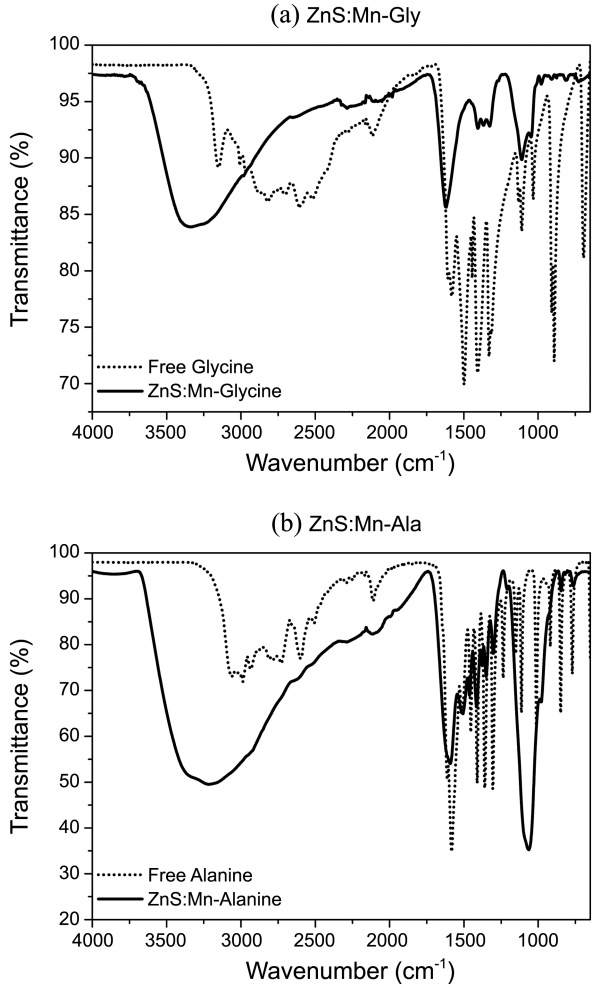

Figure 6. FT-IR spectra of: (a) ZnS:Mn-Gly and (b) ZnS:Mn-Ala nanocrystals.

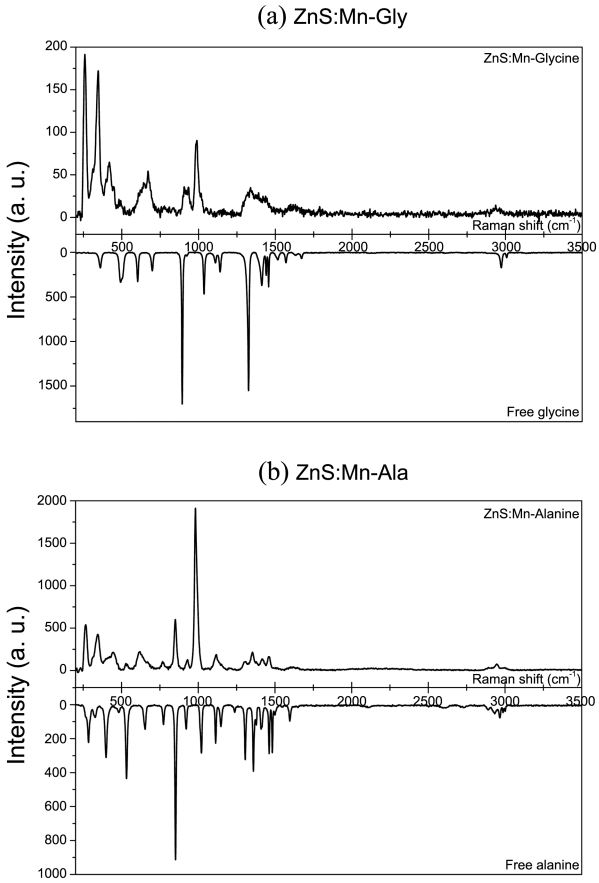

Figure 7. FT-Raman spectra of: (a) ZnS:Mn-Gly and (b) ZnS:Mn-Ala nanocrystals.

Table 2. FT-Raman data of ZnS:Mn-Gly and ZnS:Mn-Ala nanocrystals (wave numbers in cm^{-1})

ZnS:Mn-Gly	Assignments	ZnS:Mn-Ala	Assignments
259(s)	δ(NCC)	266 (s)	δ(NCC)
346(s)	Zn-S phonon	346 (m)	Zn-S phonon
418(m)	δ(CCO)/ρ(OCO)		
		448 (w)	γ(CCO)/ω(OCO)
481 (w)	δ(OCO)		
		530 (w)	ν(CN)
670 (m)	ν(CN)	620 (m)	ν(CN)
		768 (w)	ρ(CH_2)
		850 (m)	δ(CN)
906 (w)	ν(C-COO)		
989 (s)	ρ(CH_2)	982 (s)	ρ(CH_2)
		1118 (w)	ν(CC)
1338 (m)	ν(NH) + ν(OCO)	1354 (m)	ν(NH) + ν(OCO)
1391 (w)	tw(CH_2)		
		1416 (w)	tw(CH_2)
		1462 (w)	ω(CH_2)
2958 (w)		2967 (w)	ν(COO) + δ(NH)

(ν = stretching, δ = in plane bending, γ = out of plane bending, tw = twisting, ω = wagging, ρ = rocking)

scatters more scanned light, so that the intensities of the passing light decreases with the bacterial growth. Usually, spectroscopic bacterial growth monitoring is performed at a

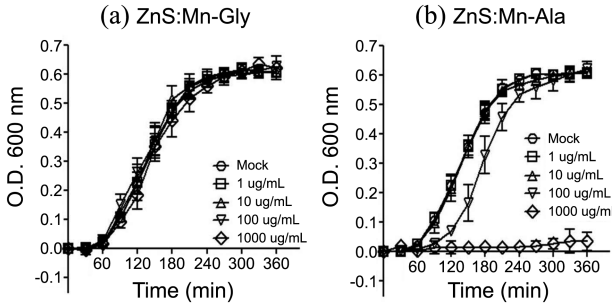

Figure 8. Effects of (a) ZnS:Mn-Gly and (b) ZnS:Mn-Ala nanocrystals on the growth of *E. coli* K-12 strain. Mock means 0 μg/mL.

working range of 550-600 nm, because the nutrient broth has a very low OD value at this wavelength region.[31] Since the ZnS:Mn nanocrystals do not emit any light in response to the scanning of the 600 nm light source, they do not interrupt the OD measurements at all. Therefore, this method is valid for estimating the biological toxicity of the amino-acid-capped ZnS:Mn nanocrystals. As shown in Figure 8, a significant degree of suppression of *E. coli* growth was observed with ZnS:Mn-Ala at concentrations of 100 μg/mL and 1 mg/mL. The difference in bacterial turbidity (O.D. 600 nm) at 5 h between the mock/low-dose group and high-dose group (100 μg/mL and 1 mg/mL) was statistically significant ($P < 0.01$). The difference at 5 hrs between the 100 μg/mL and 1 mg/mL groups was also statistically significant ($P < 0.01$), indicating that a dose-response exists in the suppression of bacterial growth. In contrast, little difference was observed in the group treated with ZnS:Mn-Gly nanocrystal. The presented maximum concentrations of the ZnS:Mn-Gly and ZnS:Mn-Ala correspond to ^{Gly}[ZnS:Mn] (3.04×10^{-8} M) and ^{Ala}[ZnS:Mn] (3.02×10^{-8} M), respectively. The concentrations of the nanocrystals in aqueous solution, represented as [ZnS:Mn], were determined by elemental analysis by ICP-AES measurements.[32] The obtained Zn and Mn concentrations were combined and converted into the nanocrystal particle concentration, assuming that the nanocrystal particle holds the same density as its bulk material. In conclusion, it can be suggested that surface capping with glycine for ZnS:Mn nanocrystal may be safer than alanine in encapsulating the toxic components of a nanocrystal. The alanine molecule contains an extra terminal methyl group, which is freely rotating in the solution state to create more molecular bulkiness than glycine. Therefore, glycine molecules on the same ZnS:Mn nanocrystal can be placed more closely to each other than alanine molecules in the capping layer of the nanocrystal. As a result, capping layer formed by the alanine molecules on the surface of the ZnS:Mn nanocrystal has more open space for the zinc atoms in the nanocrystal lattice to be dissociated from the surface to release Zn^{2+} ions, which is known as a major cause of the biological toxicity by the most nanosized inorganic semiconductor materials.[33]

Finally, in this research, we tried to investigate a relationship between aggregation effects of the nanocrystals in aqueous solvent and the observed biological toxicities. As shown

in Figure 9, the degree of aggregation of the nanocrystals in aqueous solutions was measured by a hydro-dynamic light scattering method, which showed the formation of sub-micrometer-size aggregates for both ZnS:Mn-Gly (273 ± 94 nm) and ZnS:Mn-Ala (233 ± 34 nm) in water due to the intermolecular attraction between the capping amino acid molecules. It has been shown that intermolecular interaction such as hydrogen bondings between aminoacid molecules can cause formation of aggregates with about 100 to 200 nanometer sizes in water.[34] The aminoacid molecules attached on to the different ZnS:Mn nanocrystals can also attract to each other by hydrogen bonding interaction between amino-acid-aminoacid or aminoacid-water(solvent)-aminoacid moieties. However, since alanine molecules contain an additional free-rotating methyl group from glycine, they can also cause larger van der Waals repulsion between the capping molecules on the different nanocrystals during the aggregation process. As a result, ZnS:Mn-Ala nanocrystals actually formed overall smaller-size aggregates in water even though alanine itself has bigger molecular volume than glycine. A related evidence regarding inter molecular repulsion interaction between the methyl groups in alanine molecules can be found in the previously reported crystal structure of L-alanine.[35] The packing diagram of the L-alanine crystal showed that all the methyl groups were placed far-off to each other in which the nearest distance between the methyl groups was *ca.* 700 pm, while the known van der Waals radius of methyl group is *ca.* 240 pm.[36] Even though the whole crystal structure of L-alanine makes a complicated network structure due to hydrogen bonding interactions between aminoacid molecules, the methyl groups were separated as far as possible in the solid state because of repulsive interactions between them. In addition, looking at the distribution diagrams more closely, one can also find that aggregates of ZnS:Mn-Gly are mostly formed in two different size distribution regions, which are around 100 nm and 300 nm, while aggregate distributions for the ZnS:Mn-Ala nanocrystal is mostly placed in one region (over 90% of the aggregate particles). The bigger aggregates of the ZnS:Mn-Gly reduce the surface area of the nanocrystals exposing to the bacteria. Therefore, this can also affect the toxicity of the nanocrystal over *E. coli* bacteria beside the capping effect caused by molecular volume of the individual aminoacid molecules as shown above. Even though the glycine capping layer can more tightly bound to the nanocrystal surface than that of alanine, as described above, the layer eventually causes less bulky aggregate of the ZnS:Mn nanocrystals. From this result, one can conclude that repulsion between capping layers in ZnS:Mn-Ala nanocrystals, which was majorly caused by the free rotating methyl groups, plays a critical role during the formation process of the nanocrystal aggregates in water. In another study, the determination of the degree of aggregation for a mercaptoacetic-acid-capped CdSe/ZnS core-shell quantum dot using a hydrodynamic light scattering method in aqueous solution has been reported.[37] It was found that the QD with a small size of 6.5 nm forms a larger-size (25 nm) aggregate in aqueous solution. In addition, aggregation effects of CdSe/ZnS QDs with different sizes (4.6 and 5.3 nm) at a low concentration in water, [QD] = 4.0×10^{-7} M, has also been reported.[38] Both QDs formed sub-micron aggregates and smaller QD aggregates more quickly than larger QD. Moreover, the kinetics of the aggregation of the QDs strongly depends on the nature of the surfactants. Therefore, taken together, we can conclude that the degree of aggregation for the nanocrystals associated with the nature of the surface capping agents can be critical factors affecting biological toxicity for the corresponding nanocrystal in a biological system.

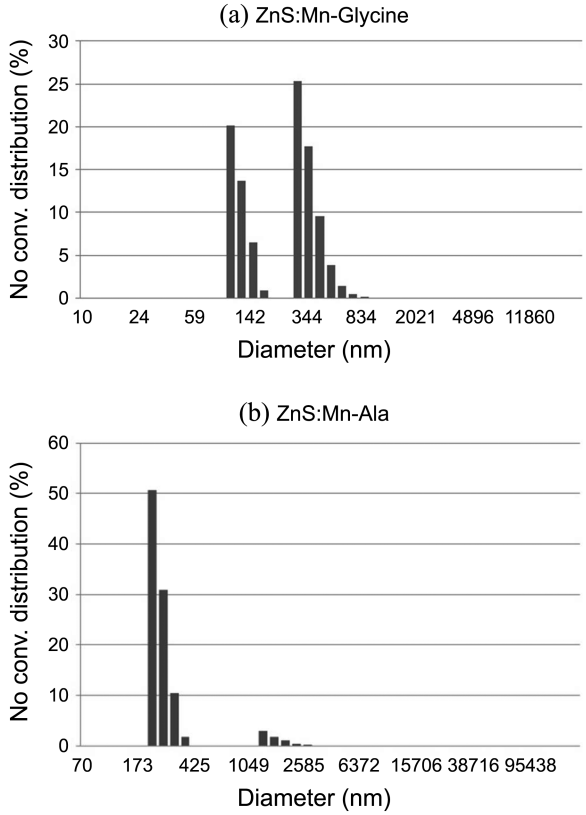

Figure 9. Particle size distribution diagrams of: (a) ZnS:Mn-Gly and (b) ZnS:Mn-Ala nanocrystals in aqueous solutions.

Conclusion

Recently, semiconductor nanocrystals have received much attention as a novel type of fluorophore for biomedical imaging. Since amino acid capping of water-soluble ZnS:Mn semiconductor nanocrystals can provide a novel platform on which to attach many biomolecules, such as DNA, RNA, and proteins, they can be used for a variety of applications, including biosensors. In this study, L-Glycine and L-Alanine-capped water-dispersible ZnS:Mn nanocrystals were successfully synthesized, and biological toxicity effects on *E. coli* were thoroughly investigated. The physical and optical properties were measured by spectroscopic methods. In the biological tests, the ZnS:Mn-Gly nanocrystal showed no significant toxicity over the growth of *E. coli* at 1000 μg/mL concentration, which is a very high dose in a biological

system scale. In general, theses water-dispersible amino acid-capped ZnS:Mn nanocrystals indeed showed sufficient physical and chemical properties suitable for biological applications. However, as demonstrated here, the degree of aggregation in water as well as the original nature of the amino acid ligands used for capping of the ZnS:Mn nanocrystals are very important factors to be considered for further applications of such nanocrystals in bio-medical areas.

Acknowledgments. This research was supported by the GRRC program in Dankook University, Gyunggi DO, Korea [GRRC-Dankook-2011-B02].

References

1. Kim, J. Y.; Voznyy, O.; Zhitomirsky, D.; Sargent, E. H. *Adv. Mater.* **2013**, *25*, 4986.
2. Choi, C. L.; Alivisatos, A. P. *Annu. Rev. Phys. Chem.* **2010**, *61*, 369.
3. Panthani, M. G.; Korgel, B. A. *Annu. Rev. Chem. Biomol. Eng.* **2012**, *3*, 287.
4. (a) Cieplak, M. *J. Phys.*: *Condens. Matter* **2013**, *25*, 190301. (b) Kairdolf, B. A.; Smith, A. M.; Stokes, T. H.; Wang, M. D.; Young, A. N.; Nie, S. *Annu. Rev. Anal. Chem.* **2013**, *6*, 143.
5. Hwang, J. M.; Oh, M. O.; Kim, I.; Lee, J. K.; Ha, C. S. *Curr. Appl. Phys*. **2005**, *5*, 31.
6. Vaksman, Y. F.; Nitsuk, Y. A.; Yatsun, V. V.; Purtov, Y. N.; Nasibov, A. S.; Shapkin, P. V. *Funct. Mater*. **2010**, *17*, 75.
7. Yu, S. H.; Wu, Y. S.; Yang, J.; Han, Z.; Xie, Y.; Qian, Y.; Liu, X. *Chem. Mater*. **1998**, *10*, 2309.
8. Gerion, D.; Pinaud, F.; Williams, S. C.; Parak, W. J.; Zanchet, D.; Weiss, S.; Alivisatos, A. P. *Phys. Chem. B* **2001**, *105*, 8861.
9. Zhang, Z. H.; Chin, W. S.; Vittal, J. J. *J. Phys. Chem. B* **2004**, *108*, 18569.
10. Jun, Y. W.; Jang, J. T.; Cheon, J. *Bull. Korean Chem. Soc.* **2006**, *27*, 961.
11. Kho, R.; Nguyen, L.; Torres-Martínez, C. L.; Mehra, R. K. *Biochem. Biophys. Res. Commun*. **2000**, *272*, 29.
12. Mitchell, G. P.; Mirkin, C. A.; Letsinger, R. L. *J. Am. Chem. Soc*. **1999**, *121*, 8122.
13. Lee, J. H.; Kim, Y. A.; Kim, K.; Huh, Y. D.; Hyun, J. W.; Kim, H. S.; Noh, S. J.; Hwang, C. S. *Bull. Korean Chem. Soc*. **2007**, *28*, 1091.
14. Hwang, C. S.; Lee, N. R.; Kim, Y. A. and Park, Y. B. *Bull. Korean Chem. Soc*. **2006**, *27*, 1809.
15. Yi. G.; Sun, B.; Yang, F.; Chen, D. J. *Mater. Chem*. **2001**, *11*, 2928.
16. Williams, A. T.; Winfield, S. A.; Miller, J. N. *Analyst* **1983**, *108*, 1067.
17. Melhuish, W. H. *J. Phys. Chem*. **1961**, *65*, 229.
18. Hasse, M. A.; Qui, J.; DePuydt, J. M.; Cheng, H. *Appl. Phys. Lett.* **1991**, *59*, 1272.
19. Lippens, P. E.; Lannoo, M. *Phys. Rev. B* **1989**, *39*, 10935.
20. Chen, W.; Su, F.; Li, G.; Joly, A. G.; Malm, J.-O.; Bovin, J.-O. *J. Appl. Phys*. **2002**, *92*, 1950.
21. Dong, B.; Cao, L.; Su, G.; Liu, W.; Zhai, H. *J. Alloys and Comp*. **2010**, *429*, 363.
22. Goswami, B.; Pal, S.; Sarkar, P. *J. Phys. Chem. C* **2008**, *112*, 11630.
23. *International Union of Crystallography in International Tables for X-ray Crystallography, Part III*; Netherlands, Dordrecht, 1985; p 318.
24. Kushida, T.; Tanak, Y.; Oka, Y. *Sol. Stat. Commun*. **1974**, *14*, 617.
25. Fischer, G.; Cao, X.; Cox, N.; Francis, M. *Chem. Phys*. **2005**, *313*, 39.
26. Kumar, S.; Rai, A. K.; Rai, S. B.; Rai, D. K.; Singh, A. N.; Singh, V. B. *J. Mol. Struct*. **2006**, *791*, 23.
27. Dumane, N. R.; Hussaini, S. G.; Dongre, V. G.; Ghugare, P.; Shirsat, M. D. *Appl. Phys. A* **2009**, *95*, 727.
28. Moszczenski, C. W.; Hooper, R. J. *Inorg. Chim. Acta* **1983**, *70*, 71.
29. Schneider, J.; Kirby, R. D. *Phys. Rev. B* **1972**, *6*, 1290.
30. Begot, C.; Desnier, I.; Daudin, D. J.; Labadie, J. C.; Lebert, A. *J. Microbiol. Meth*. **1996**, *25*, 225.
31. Zabic, M.; Kukric, Z.; Topalic-Trivunovic, L. *Chem. Ind. & Chem. Eng. Quart*. **2009**, *15*, 251.
32. Yu, W. W.; Qu, L.; Guo, W.; Peng, X. *Chem. Mater*. **2003**, *15*, 2854.
33. (a) Huang, Y. W.; Wu, C. H.; Aronstam, R. S. *Materials* **2010**, *3*, 4842. (b) Hardman, R. *Environ. Health Perspect*. **2006**, *114*, 165.
34. Hagmeyer, D.; Ruesing, J.; Fenske, T.; Klein, H. W.; Schmuck, C.; Schrader, W.; Piedade, M. E.; Epple, M. *RCS Adv.* **2012**, *2*, 4690.
35. Marsh, R. E.; Simpson, H. J. *Acta Crysatllogr.* **1966**, *20*, 550.
36. Schiemenz, G. P. *Z. Naturforsch* **2007**, *62b*, 235.
37. Kim, J. W.; Han, J. J.; Choi, J. G.; Kim, D. K.; Je, K. C.; Park, S. H.; Yun, J. I.; Fanghanel, T. *J. Kor. Phys. Soc*. **2006**, *49*, 135.
38. Korala, L.; Stephanie, L. B. *J. Phys. Chem. C* **2012**, *116*, 17110.